J Appl Electrochem (2008) 38:1301–1311
DOI 10.1007/s10800-008-9557-8

ORIGINAL PAPER

Evaluation of some bipyridinium dihalides as inhibitors for low carbon steel corrosion in sulfuric acid solution

M. S. Morad · A. A. Hermas · A. Y. Obaid · A. H. Qusti

Received: 16 December 2007 / Revised: 25 March 2008 / Accepted: 31 March 2008 / Published online: 29 April 2008

Abstract Inhibition of low carbon steel (LCS) corrosion in 0.5 M H_2SO_4 solution by three bipyridinium dihalides ($TMbPyBr_2$, $HMbPyBr_2$ and $MPhbPyCl_2$) was evaluated by potentiodynamic polarization curves, EIS and SEM techniques. The effectiveness of the inhibitors is ranked as follows: $MPhbPyCl_2 \cong TMbPyBr_2 > HMbPyBr_2$. The compounds behave as mixed-type inhibitors and their adsorption on the steel surface obeys the Langmuir adsorption isotherm. EIS measurements indicate that charge transfer controls the corrosion of steel in the absence and presence of the inhibitors and the equivalent circuit $R_e(R_{ct}Q_{dl})$ represents the electrode/solution interface either at the corrosion potential or at −75 and 30 mV versus E_{corr}. The compounds show maximum inhibition efficiency at 35 °C. The mechanism of corrosion inhibition was discussed in the light of the molecular structure of the bipyridinium salts.

Keywords Adsorption · Bipyridinium salts · Corrosion inhibition · Low carbon steel · EIS

M. S. Morad (✉)
Electrochemistry Research Laboratory, Chemistry Department, Faculty of Science, Assiut University, 71516 Assiut, Egypt
e-mail: morad60@aun.edu.eg; mmorad04@yahoo.com

A. A. Hermas
Chemistry Department, Faculty of Science, Assiut University, Assiut, Egypt

A. A. Hermas · A. Y. Obaid · A. H. Qusti
Chemistry Department, Faculty of Science, King Abdulaziz University, Jeddah, Saudi Arabia

1 Introduction

The influence of various aliphatic and aromatic quaternary ammonium salts on the corrosion of iron and steel in acid solutions has been extensively studied [1–8]. It is well known that the heterocyclic systems, bearing quaternized nitrogen atom, have better corrosion inhibition than the alkyl substituted quaternary ammonium compounds [4]. It has been reported that the inhibiting action of quaternary salts of pyridinium bases increases with increase in the carbon chain length substituted at the nitrogen atom [1]. The inhibitory effect of N-decyl pyridinium derivatives on the dissolution of iron in HCl and H_2SO_4 solutions has been studied by some workers [3]. Electrochemical measurements were employed to test the performance of n-cetylpyridinium chloride (CPC) as inhibitor for low carbon steel corrosion in sulfuric acid solution [5]. CPC showed excellent inhibition effect (up to 97%) and its adsorption on the steel surface followed Bockris–Swinkels isotherm. Popova et al. [7, 8] investigated four quaternary ammonium bromides of different heterocyclic compounds as corrosion inhibitors of mild steel in 1 M HCl and 1 M H_2SO_4. They found that the inhibitors are of mixed type and influencing predominantly the anodic process. Several tetra-alkyl ammonium hydroxides have been recently proposed and testified as novel inhibitors of Zn dendrite and Zn-based secondary batteries to replace the well-known tetra-alkyl ammonium bromides [9]. The ability to inhibit Zn dendrite was found dependent on the size of alkyl group and that the rechargeability of Zn anode is highly improved by the introduction of the proposed additives.

Most of the previous studies concerned the organic compounds that containing one quaternary nitrogen atom. Few studies [10–15] were found in the literature where the onium compound contains two nitrogen atoms.

1,10-Ethylene-bispyridinium halides and its substituted compounds have been investigated as pickling inhibitors for mild steel in HCl and H_2SO_4 solutions [10, 11]. The Gemini surfactants 1,2-ethylene bis[dimethyl alkyl (C_nH_{2n+1}), n = 10, 12 and 16] ammonium dibromides were tested as inhibitors for mild steel corrosion in HCl solution [12, 13]. The inhibiting action of the surfactants was attributed to their adsorption on the steel surface which followed Langmuir isotherm. Yao et al. [14] recently studied the inhibitive effect of a new type of Gemini surfactant (cationic Gemini with pyridinium) on the corrosion of iron in HCl solution. It was found that 1,4/1,6-bis (α-octylpyridinium) butane/hexane dibromide acts as a mixed type inhibitor as a result of the formation of a protective layer on the iron surface. Aziz et al. [15] investigated the n-methylated-dipyridinium iodide as inhibitors for Zn corrosion in HCl solution. Among the compounds, N,N-dimethyl-4,4'-dipyridinium diiodide was found to be the most efficient one.

In this paper, the inhibition effect of three substituted bipyridinium dihalides was investigated. The type and the number of substituents were varied in order to check the influence of molecular structure on the behaviour of the inhibitor. Potentiodynamic polarization, electrochemical impedance spectroscopy (EIS) and scanning electron microscopy were employed.

2 Experimental details

2.1 Synthesis of bipyridinium dihalide derivatives

Three bipyridinium dihalide derivatives whose chemical structures are shown in Fig. 1 were synthesized as follows.

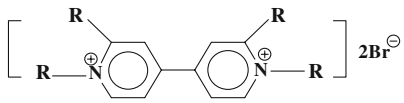

1, 1', 2, 2'- tetramethyl-4, 4'-bipyridinium dibromide ($TMbPyBr_2$)

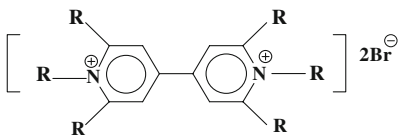

1, 1', 2, 2', 6, 6'- hexamethyl-4, 4'-bipyridinium dibromide ($HMbPyBr_2$)

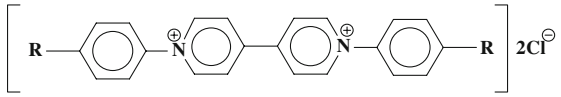

1, 1'-bis(4-methylphenyl)4, 4'-bipyridinium dichloride ($MPhbPyCl_2$)

Fig. 1 Structure of bipyridinium dihalide derivatives. In all cases, R = $-CH_3$

1,2-dimethylpyridinium bromide was firstly prepared by reacting of α-picoline with methyl bromide, the product was recrystallized from ethanol. A solution of pyridinium salt (1.5 g) in 1,2-diaminoethane (10 mL) was stirred for 30 min under an atmosphere of nitrogen and then treated with sodium cyanide (0.3 g). The precipitate was collected after 24 hours and washed several time with distilled water. The cyanide-free product was then oxidized by dissolving in bromine water to give a yellow solution of $TMbPyBr_2$. The aqueous solution was concentrated by evaporation in a water bath and the product was then precipitated by adding an excess of acetone. Further recrystallization from ethanol gives the product as fine crystals (yield = 1.35 g, 55.33%). Starting with 2,6- lutidine, $HMbPyBr_2$ was prepared by the same procedure [16]. $MPhbPyCl_2$ was synthesized according to Evan et al. [17]. The compounds were characterized using melting points, elemental analysis and ^{1}HNMR.

2.2 Electrodes, electrolytes and additives

A LCS sample of the following chemical composition (as w%) served as working electrode:

C	P	S	Si	Mn	Cr	Ni	Cu	Fe
0.18	0.01	0.025	0.014	0.32	0.04	0.035	0.08	Rest

A LCS cylinder pressed in a Teflon holder acted as a working electrode. Its working area was 0.196 cm^2. A saturated calomel electrode (SCE) and a platinum sheet of large surface area were served as reference and auxiliary electrodes respectively. To avoid contamination with Cl^- ion, the SCE was coupled to a Luggin capillary filled with 0.5 M H_2SO_4 solution. The tip of the Luggin capillary was located very close to the working electrode (~1 mm distance) [18].

Prior to each experiments the working electrode was wet polished with emery papers up to grade 600, rinsed with bi-distilled water, acetone, bi-distilled water and transferred wet to the glass cell , filled already with 200 mL of 0.5 M H_2SO_4 solution. The latter was deaerated by purified nitrogen during 1 h prior to the insertion of the working electrode and purging with nitrogen continued during the course of the experiments.

0.5 M H_2SO_4 solution was prepared from concentrated H_2SO_4 (Merck) and bi-distilled water. The inhibitor solution was prepared by dissolving the appropriate weight in 0.5 M H_2SO_4 solution .All experiments were conducted in stirred solutions.

It is worth mentioned that each electrochemical test was repeated at least twice and the experimental results are reasonably reproducible within the limits of the experimental error (≤5%).

2.3 Instrumentation

The EG&G instruments electronic equipment was used. It included a PAR Model 273 potentiostat/galvanostat and a 5210 two-phase lock-in analyzer. Potentiodynamic polarization curves (Tafel plots) were conducted with a scan rate of 0.2 mV/sec in the potential range −200 to +125 mV from the corrosion potential (E_{corr}).

EIS measurements were taken from 100 mHz to 100 kHz and peak to peak ac amplitude of 5 mV with 5 points per decade.

The impedance spectra were collected at three polarization potentials, namely, E_{corr}, −75 mV and 30 mV versus E_{corr}. EQUIVCRT commercial software [19] was used to fit the impedance data.

Both polarization curves and impedance measurements were monitored by an IBM personal computer via a GBIP–IIA interface. The standard programs M352/252 and M398 were used for collecting the experimental data.

Examination of the morphology of the steel surface in sulfuric acid solution without and with some selected concentrations of the studied bipyridinium compounds was achieved using scanning electron microscopy (JSM 5400 LV).

3 Results and discussion

3.1 Open circuit corrosion potential (OCP) versus time measurements

Variation of the OCP of the working electrode as a function of time plays an important role in defining domains of corrosion, partial or complete inhibition and in determining the inhibitor threshold concentration [20]. Figure 2 represents the variation of the steel electrode with time in 0.5 M H_2SO_4 solution without and with different concentrations of $TMbPyBr_2$ (Fig. 2a), $HMbPyBr_2$ (Fig. 2b) and $MPhbPyCl_2$ (Fig. 2c) respectively. At the moment of immersion of the steel electrode in the pure acid solution, a potential of ca −558 mV versus SCE was recorded. This changed quickly towards more positive values giving rise to a clear arrest which corresponds to the free corrosion potential (E_{corr}) of −526 mV versus SCE after 400 s. The positive shift of OCP in the blank solution can be attributed to the mass transport effect which results from the removal of any oxide layer and/or adsorbed species [21]. It was reported that in the oxidation reaction, the overall mechanism may be rate limited by diffusion of both product layer formation and dissolution [22]. In presence of the investigated bipyridinium salts, different features could be observed. Addition of 10 μM $TMbPyBr_2$ (Fig. 2a) moves the steady state corrosion potential in the negative direction. Further additions

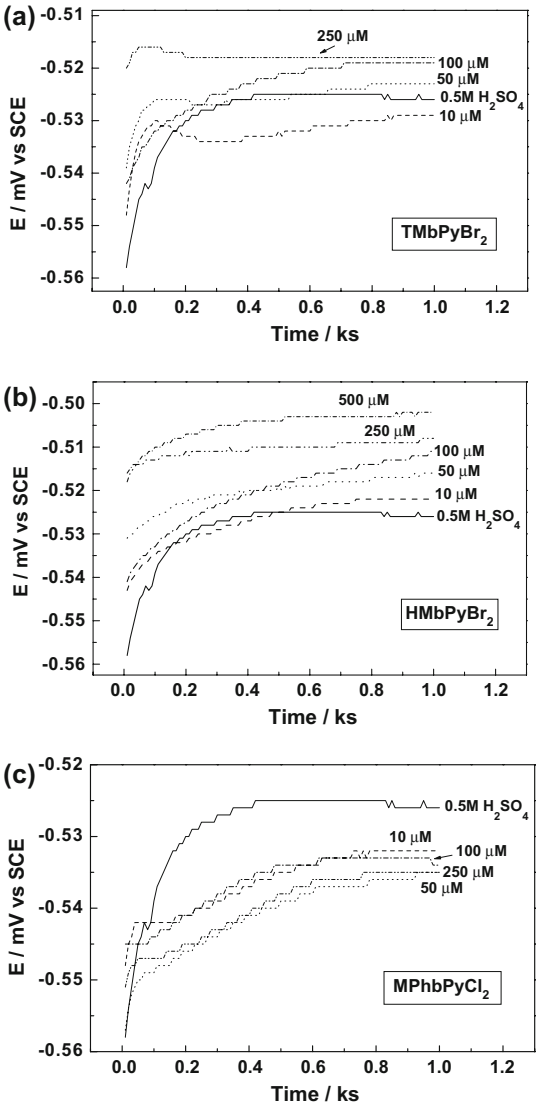

Fig. 2 Potential–time curves of mild steel corrosion in 0.5 M H_2SO_4 solution in absence and presence of: (**a**) $TMbPyBr_2$ (**b**) $HMbPyBr_2$ (**c**) $MPhbPyCl_2$

shift E_{corr} towards nobler values compared to that of the blank solution. In the case of $HMbPyBr_2$ (Fig. 2b), values of E_{corr} are more positive than that recorded in the pure medium and the positive shift is increased with increasing additive concentration. Values of E_{corr} obtained in the presence of $MPhbPyCl_2$ (Fig. 2c) are shifted towards more active values and the maximum shift is observed at 50 μM concentration. In the presence of the additive, the shift of E_{corr}, obtained in the pure medium, in the negative (less noble values) direction indicates that the inhibitor mainly influences the cathodic reaction (hydrogen evolution) while the positive shift (more noble values) indicates that the inhibitor mainly influences the anodic reaction (steel dissolution) [23] though the additives behave as a whole as inhibitors of mixed type (see below).

3.2 Polarization curves at 35 °C

Figure 3 shows typical anodic and cathodic potentiodynamic polarization curves at 35 °C in 0.5 M H_2SO_4 in the presence of various concentration of $TMbPyBr_2$. (Representative curves). Comparison of the curves shows that with respect to the blank, increasing the concentration of the additive gave rise to a consistent decrease in both cathodic and anodic current densities up to 100 μM concentration indicating the inhibition of both hydrogen evolution and steel dissolution reactions. The influence of $TMbPyBr_2$ on the cathodic reaction is more pronounced. Accordingly, $TMbPyBr_2$ can be considered as inhibitor of mixed type with a dominant effect on the cathodic reaction. At 250 μM, an increase in the anodic and cathodic current densities is observed indicating the loss of the inhibition efficiency at the highest examined concentration. Addition of $TMbPyBr_2$ gives rise to polarization curves run parallel to that of the blank solution. So, $TMbPyBr_2$ does not alter the mechanism of either hydrogen evolution or steel dissolution reactions. Both $HMbPyBr_2$ and $MPhbPyCl_2$ show the same behaviour as that of $TMbPyBr_2$ with the difference that the anodic reaction is much more inhibited than the cathodic one in case of $HMbPyBr_2$.

Values of corrosion current density (i_{corr}) associated with the polarization curves of Fig. 3 and those obtained in the presence of $HMbPyBr_2$ and $MPhbPyCl_2$ were calculated by extrapolation of both anodic and cathodic branches of the polarization curve (within Tafel regions) back to E_{corr}. The electrochemical parameters, namely corrosion current density (i_{corr}), cathodic ($-\beta_c$) and anodic (β_a) Tafel slopes, were calculated. In 0.5 M H_2SO_4 solution, the value of i_{corr} was found to be 1986 μA cm^{-2}. This value decreases in the presence of the additives. The maximum decrease is obtained at 100 μM $TMbPyBr_2$ (154 μA cm^{-2}), 500 μM $HMbPyBr_2$ (977 μA cm^{-2}) and at 100 μM $MPhbPyCl_2$ (145 μA cm^{-2}). On the other hand, values of β_a and β_c obtained in the absence and presence of investigated bipyridinium salts were found to be 50 ± 5 and −115 ± 5 mV/decade respectively. Values of i_{corr} were used to calculate the inhibition efficiency (IE%) of the additives according to:

$$IE\% = \left\{ \left[i^{o}_{corr} - i_{corr} \right] / i^{o}_{corr} \right\} \times 100 \quad (1)$$

where i^{0}_{corr} and i_{corr} are corrosion current density in the absence and presence of the inhibitor respectively. The dependence of IE% on the concentration for all inhibitors is presented in Fig. 4. For all inhibitors, values of IE% increase with increasing the concentration reaching a maximum at 100 μM $TMbPyBr_2$ and $MPhbPyCl_2$ and at 500 μM $HMbPyBr_2$. According to the maximum inhibitor efficiency, the inhibitors are ranked as follows:

$$MPhbPyCl_2(92.7\%) \cong TMbPyBr_2(92.2\%) \gg HMbPyBr_2(50.8\%).$$

3.3 Adsorption isotherms

The action of an inhibitor in aggressive acid media is assumed to be due to its adsorption at the metal/solution interface. The adsorption process depends on the electronic characteristics of the inhibitor, the nature of metal surface, temperature, steric effects and the varying degrees of surface-site activity [24]. The adsorption of an organic adsorbate at a metal/solution interface can be regarded as a substitution adsorption process between the organic molecule in the aqueous solution $Org_{(sol)}$ and the water molecules on the metallic surface $H_2O_{(ads)}$ [25]:

$$Org_{(sol)} + x\ H_2O_{(ads)} \rightleftarrows Org_{(ads)} + x\ H_2O_{(sol)} \quad (2)$$

x is the size ratio representing the number of water molecules replaced by a molecule of organic adsorbate.

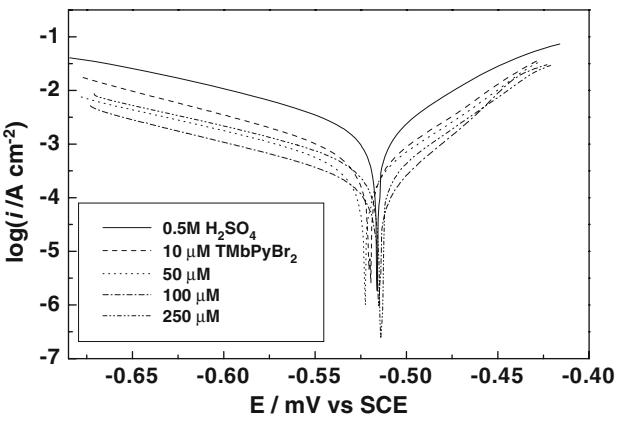

Fig. 3 Potentiodynamic polarization curves obtained at 35 °C for mild steel corrosion 0.5 M H_2SO_4 solution in absence and presence of $TMbPyBr_2$

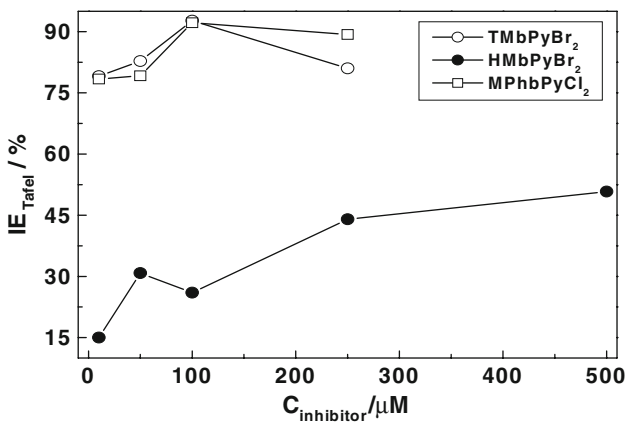

Fig. 4 Variation of the inhibition efficiency (deduced from polarization curves) with the concentration of the bipyridinium salts

In an attempt to find the most suitable adsorption isotherm(s), the fraction of surface coverage (θ), which was calculated from the equation:

$$\theta = \left[1 - \left(i_{corr}/i^{o}_{corr}\right)\right] \quad (3)$$

was subjected to various adsorption isotherms. For all compounds, the experimental results were found to fit Langmuir adsorption isotherm where θ and C (inhibitor concentration in the bulk of the solution) are related to each other via the equation:

$$\theta = KC/(1 + KC) \quad (4)$$

Rearrangement gives:

$$C/\theta = (1/K) + C \quad (5)$$

where K is the equilibrium constant of the adsorption process. Figure 5 shows a plot of C/θ against C where straight lines are obtained. For $TMbPyBr_2$ and $MPhbPyCl_2$, the slope of the straight line is nearly equal to unity while the straight line obtained in the case of $HMbPyBr_2$ has a slope >1. So, it can be concluded that $TMbPyBr_2$ and $MPhbPyCl_2$ are adsorbed at the steel surface following Langmuir isotherm without interaction between the adsorbed molecules. In the case of $HMbPyBr_2$, deviation of the slope from unity can be explained in terms of repulsion or attraction of the adsorbed molecules adjacent to each other, a fact which was ignored during the derivation of the Langmuir isotherm [18]. The interaction between $HMbPyBr_2$ molecules can be ascribed to the steric hindrance exerted by the six methyl groups.

The constant K is related to the standard to the standard free energy of adsorption (ΔG^{o}_{ads}) by the equation:

$$K = (1/55.5)\exp\left(-\Delta DG^{o}_{ads}/RT\right) \quad (6)$$

Values of K were found as 2.165×10^5, 6.58×10^3, and 4.98×10^5 M^{-1} for $TMbPyBr_2$, $HMbPyBr_2$ and $MPhbPyCl_2$ respectively. The increasing value of K from $HMbPyBr_2$ to $MPhbPyCl_2$ reflects the increasing adsorption capability on the steel surface [26]. Values of ΔG^{o}_{ads} were found to be −41.1, −32.26 and −43.2 kJ mol^{-1} for $TMbPyBr_2$, $HMbPyBr_2$ and $MPhbPyCl_2$ respectively. Generally, values of ΔG^{o}_{ads} around −20 kJ mol^{-1} or lower are consistent with electrostatic interaction between the charged molecules and the charged metal surface (physisorption) while those around −40 kJ mol^{-1} or higher involve charge sharing or charge transfer from the organic molecules to the metal surface to form a coordinate type bond (chemisorption) [27]. Values of ΔG^{o}_{ads} between −20 and −40 kJ mol^{-1} indicate that the adsorption mechanism involves two types interaction, physisorption and chemisorption [28]. In the light of the above criteria, both $TMbPyBr_2$ and $MPhbPyCl_2$ are chemisorbed on the steel surface while adsorption of $HMbPyBr_2$ involves two processes, physisorption and chemisorption. Comparing ΔG^{o}_{ads} values, the investigated bipyridinium salts are ranked as follows: $MPhbPyCl_2 > TMbPyBr_2 > HMbPyBr_2$.

3.4 Impedance measurements at 35 °C

Figure 6 shows Nyquist plots (representative spectra) recorded for the corrosion of LCS in H_2SO_4 solution without and with 1–250 μM $MPhbPyCl_2$ obtained at E_{corr}. Whatever the concentration, the impedance diagrams display a single depressed capacitive loop covering most of the frequency range and a small inductive loop appears at very low frequency values. The capacitive loop is related to the charge transfer process of the metal corrosion and the double layer behaviour. The inductive loop may be attributed to the relaxation of adsorbed species $[FeOH]_{ads}$ and $[FeH]_{ads}$ in the case of the blank solution, while adsorption of the inhibitor molecules or ion on the steel surface may explain the appearance of the inductive loop in the presence of the inhibitors [29]. At 100 and 250 μM

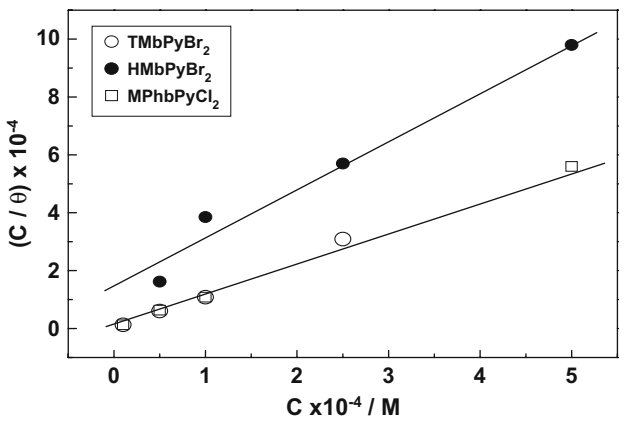

Fig. 5 Langmuir adsorption isotherms of bipyridinium salts on mild steel electrode in 0.5 M H_2SO_4

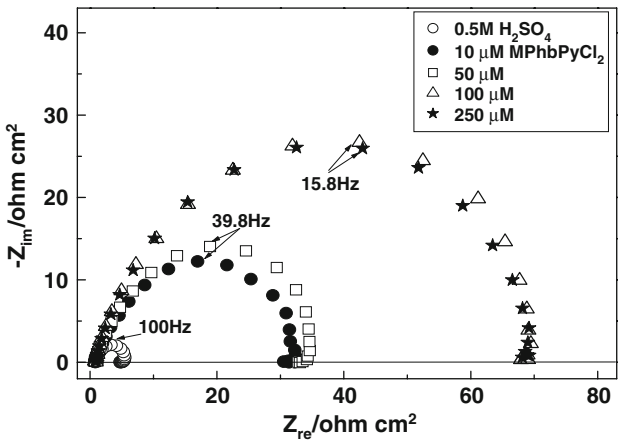

Fig. 6 Typical Nequist plots of mild steel electrode recorded at E_{corr} in 0.5 M H_2SO_4 solution without and with $MPhbPyCl_2$, t = 35 °C

concentrations, the inductive loop is not so remarkable. A depressed semicircle may be attributed to different physical phenomena such as roughness and surface inhomogeneities, impurities, grain boundaries and distribution of the surface active sites [30]. The addition of $MPhbPyCl_2$ did not change the general shape of the semicircles but a large increase in their radii is observed upon increasing the concentration of $MPhbPyCl_2$ up to 100 μM before decreasing again at 250 μM. The results indicate that the maximum inhibition effect for this compound is obtained at 100 μM. Similar results were obtained in the presence of $TMbPyBr_2$ and $HMbPyBr_2$.

The impedance parameters, namely charge transfer resistance (R_{ct}), the constant phase element (Q_{dl}) related to the capacity of the double layer and relevant to the capacitive semicircle of the LCS/H_2SO_4/$MPhbPyCl_2$ system were calculated from the non-linear Least Squares Fit (NLSF) of the equivalent circuit [18]. Values of R_{ct} and Q_{dl} obtained in the pure medium were found to be 4.8 Ω cm^2 and 5.4 × 10^{-4} $Ω^{-1}$ cm^{-2} s^n respectively. As the additive concentration increases, R_{ct} (and hence values of IE%) increase, reaching a maximum value of 69.7 Ω cm^2 (IE% = 93.1) at 100 μM concentration. On the other hand, the value of Q_{dl} obtained in the pure medium is reduced by ~43–60%. The increase in R_{ct} and the decrease in Q_{dl} with increasing concentration indicate that $MPhbPyCl_2$ acts as a primary interface inhibitor and that charge transfer controls the corrosion of mild steel under the open circuit conditions. On the other hand, the decrease in Q_{dl}, which can result from a decrease in the local dielectric constant and/or an increase in the thickness of the electrical double layer, suggest that $MPhbPyCl_2$ functions by adsorption at the metal/solution interface [31].

Values of R_{ct} were used to calculate the inhibition efficiency of $TMbPyBr_2$, $HMbPyBr_2$ and $MPhbPyCl_2$ according to:

$$IE\% = \left\{\left[R_{ct} - R_{ct}^{\circ}\right]/R_{ct}\right\} \times 100 \quad (7)$$

where R_{ct}^{o} and R_{ct} are values of charge transfer resistance in the absence and presence of additive respectively. Figure 7 show the dependence of the inhibition efficiency on the concentration of the bipyridinium salts. For both $TMbPyBr_2$ and $MPhbPyCl_2$, the maximum value of IE% is obtained at 100 μM, while $HMbPyBr_2$ shows maximum efficiency at 250 μM. According to the maximum IE%, the inhibitors follow the order: $MPhbPyCl_2 \cong TMbPyBr_2 > HMbPyBr_2$ which is in good agreement with the results from the polarization curves. The inhibition efficiency of $HMbPyBr_2$ calculated from EIS is relatively higher than that from the polarization curves. This discrepancy may be attributed to the state of the electrode surface. EIS is classified as a non-destructive (non-invasive) technique [32] where the state of the electrode surface

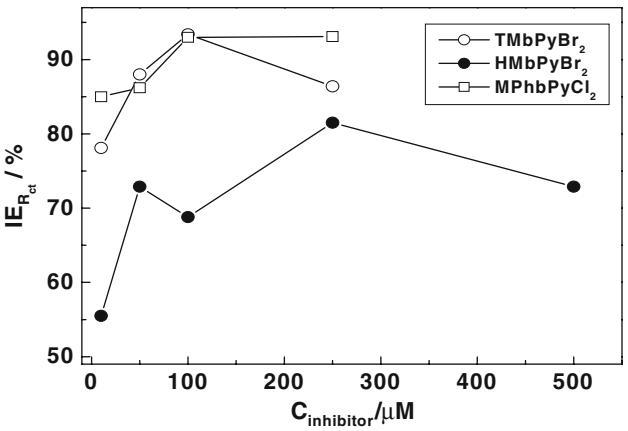

Fig. 7 Variation of the inhibition efficiency (deduced from R_{ct} values obtained at E_{corr}) with the concentration of the bipyridinium salts

is practically unchanged, while polarization greatly influences the surface state and hence the adsorption process.

To ensure the validity of the results obtained from the polarization curves, impedance measurements were also performed at two potentials, −75 and 30 mV versus E_{corr}. Figures 8 and 9 show the Nyquist plots. These spectra were recorded only for the concentrations at which the inhibitor shows its maximum inhibition efficiency. The figures demonstrate that the presence of the additives did not alter the general shape of the spectrum obtained in the blank solution indicating no change in the mechanism of both hydrogen evolution and steel dissolution reactions. Disregarding the small capacitive loop in the low frequency region of Fig. 8 and the inductive loop of Fig. 9, calculation of the impedance parameters according to the proposed equivalent circuit model is still valid. At both polarization potentials, impedance spectra provide further evidence that the bipyridinium dihalides are inhibitors of mixed type. Values of the inhibition efficiency deduced

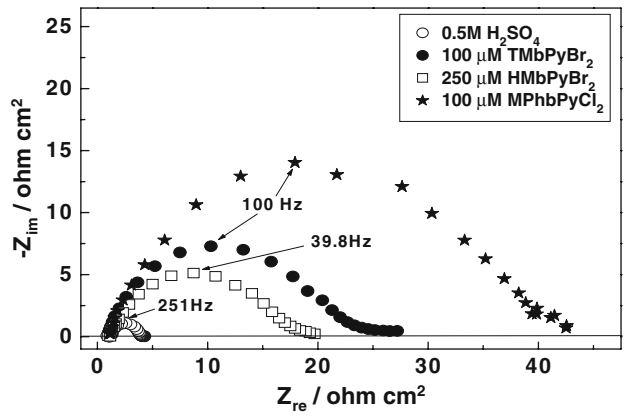

Fig. 8 Typical Nequist plots of mild steel electrode recorded at −75 mV versus E_{corr} in 0.5 M H_2SO_4 solution without and with the inhibitor concentration at which IE% is maximum, t = 35 °C

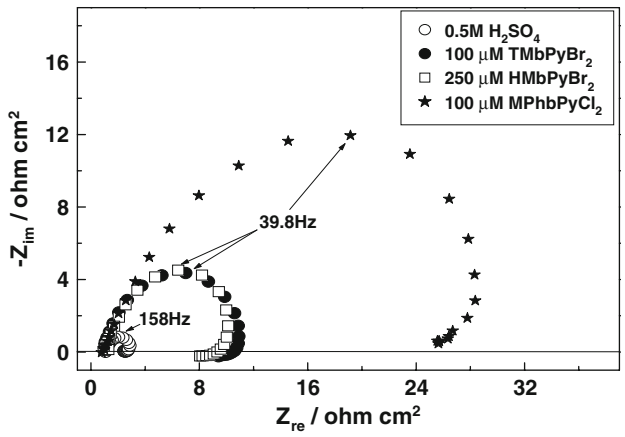

Fig. 9 Typical Nequist plots of mild steel electrode recorded at 30 mV versus E_{corr} in 0.5 M H_2SO_4 solution without and with the inhibitor concentration at which IE% is maximum, t = 35 °C

Table 1 Values of IE% calculated from R_{ct} obtained at different polarization potentials for the system mild steel/0.5 M H_2SO_4 in presence of bipyridinium dihalides at 35 °C

$C_{inhibitor}$ (μM)	At −75 mV versus E_{corr}	At 30 mV versus E_{corr}
100 μM $TMbPyBr_2$	86	80.6
250 μM $HMbPyBr_2$	82.8	75.4
100 μM $MPhbPyCl_2$	92.3	93.4

from Figs. 8 and 9 according to Eq. 7 are shown in Table 1, indicating that $MPhbPyCl_2$ is the most efficient compound. The ranking is $MPhbPyCl_2$ > $TMbPyBr_2$ > $HMbPyBr_2$.

3.5 Scanning electron microscopy (SEM)

Figure 10 shows the scanning electron micrographs of LCS after immersion for 10 min in deaerated 0.5 M H_2SO_4 without and with $TMbPyBr_2$ and $MPhbPyCl_2$ (250 μM for each) at 35 °C. The image of the surface exposed to the inhibitor-free solution (Fig. 10a) appears to be roughened extensively (general corrosion with localized attack) by the corrosive medium. In the presence of 250 μM of $TMbPyBr_2$, the surface (Fig. 10b) is practically clean with the appearance of some white deposits distributed in a random way over the whole electrode surface. The micrograph obtained in the presence of 250 μM of $MPhbPyCl_2$ (Fig. 10c) is the same as that of Fig. 10b but the white deposits are notable and cover the whole surface. The surface topography becomes corrugated mainly due to the formation of a complex morphology resembling a cellular distribution of flakes, some of them gathering in more dense formations. The roughness pattern due to the surface preparation process previous to immersion is still visible in Fig. 10b, c. The results indicate that $MPhbPyCl_2$ provides better inhibition performance than $TMbPyBr_2$. To ensure that the electrode surface is free from corrosion, the white deposits appearing in Fig. 10c were removed and another image was recorded (Fig. 10d). The electrode surface appears to be free from corrosion (general and localized) and the white deposits are more pronounced than those of Fig. 10b. The marked decrease in the corrosive attack may be attributed to adsorption of the inhibitors. Adsorption of $MPhbPyCl_2$ is greater than that of

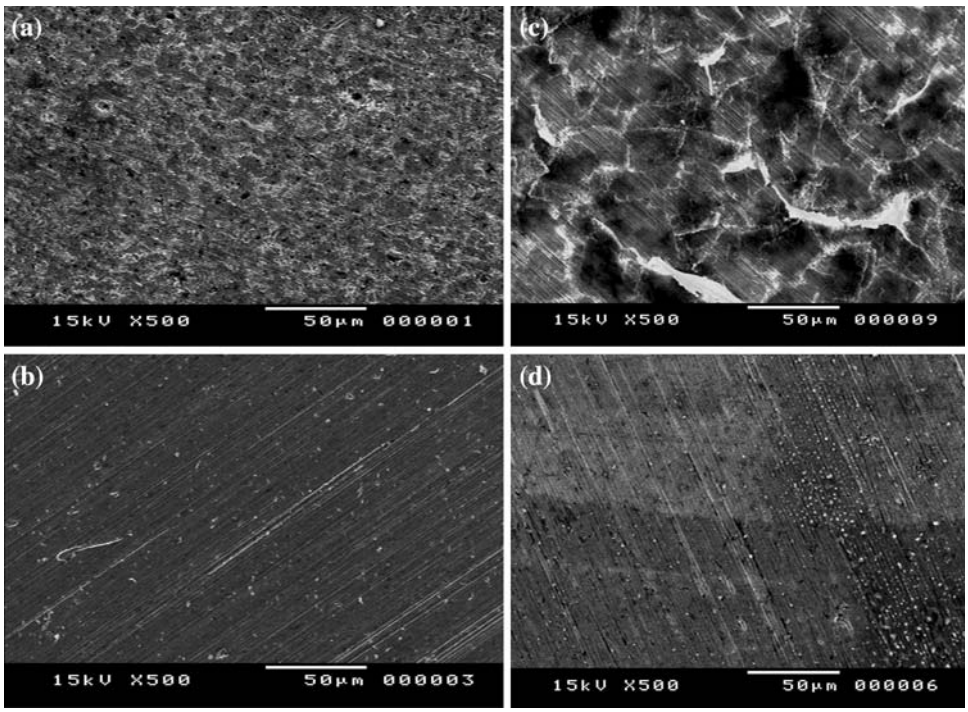

Fig. 10 Scanning electron micrographs of mild steel surface(immersion time = 10 min, t = 35 °C): (**a**) in 0.5 M H_2SO_4 solution. (**b**) in presence of 250 μM $TMbPyBr_2$ (**c**) in presence of 250 μM $MPhbPyCl_2$ (**d**) in presence of 250 μM MPhbPyCl2 after removal of the inhibitor ($MPhbPyCl_2$) layer

$TMbPyBr_2$. SEM results are in good agreement with those obtained from polarization curves (Fig. 4) and EIS (Fig. 7).

4 Effect of temperature

4.1 Polarization curves

The effect of temperature on the inhibited acid-metal reaction is complex, because many changes occur on the metal surface. These changes may involve rapid etching and desorption of the inhibitor or the inhibitor itself may undergo decomposition and/or rearrangement. Polarization curves (not shown here) were recorded at 25, 30 and 40 °C for the concentrations which gave the best inhibition efficiency at 35 °C. Values of i_{corr} deduced from these curves are lower at 25 and 30 °C than that obtained at 35 °C while that obtained at 40 °C is higher. The inhibition efficiency was calculated from Eq. 1 and is plotted as a function of temperature in Fig. 11. Values of IE% show an initial decrease at 30 °C, reaching a maximum at 35 °C before decreasing again at 40 °C. At the later temperature, the decrease in inhibition efficiency follows the order: $HMbPyBr_2 > TMbPyBr_2 > MPhbPyCl_2$. On the other hand, the dependence of corrosion current density on the temperature can be expressed by the Arrhenius equation:

$$\log i_{corr} = \log \lambda - (E_a/2.303\ RT) \quad (8)$$

λ is the pre-exponential factor and E_a is the apparent activation energy of the corrosion process. Arrhenius plots obtained for the corrosion of mild steel in the uninhibited and inhibited acid solutions are shown in Fig. 12. Values E_a were calculated by regression between log i_{corr} and (1/T). The linear regression coefficient in all cases was found to be >0.98. These values were found to be 64.3, 72, 119.8 and 56.6 kJ mol^{-1} for the blank solution, $TMbPyBr_2$, $HMbPyBr_2$ and $MPhbPyCl_2$

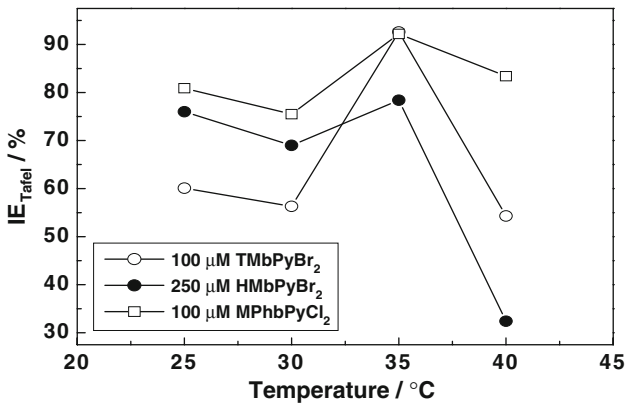

Fig. 11 Variation of the inhibition efficiency (deduced from polarization curve) of the bipyridinium salts at concentrations of maximum IE% with the temperature

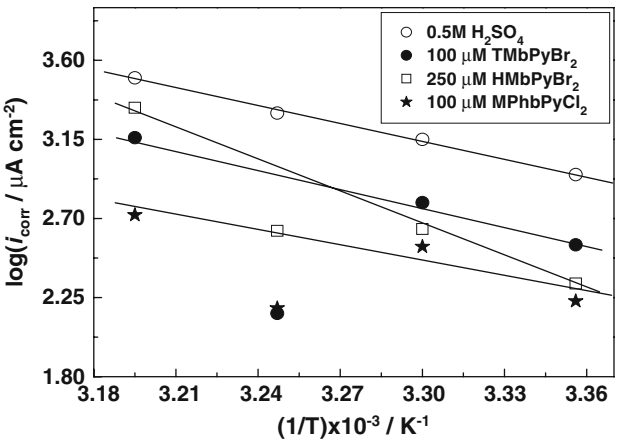

Fig. 12 Arrhenius plots of mild steel corrosion in 0.5 M H_2SO_4 solution in absence and presence of concentrations of bipyridinium salts at which IE% is maximum

respectively. The value of 64.3 kJ mol^{-1} obtained for the activation energy of the corrosion process in 0.5 M H_2SO_4 solution lies in the range of the most frequently cited values, the majority of which are grouped around 60 kJ mol^{-1} [33]. The lower value of apparent activation energy obtained in the presence of $MPhbPyCl_2$ can be attributed to surface chemisorption [34, 35]. Hoar and Holliday [36] attributed the decrease in activation energy of the corrosion process in the inhibited state to the slow rate of inhibitor adsorption with a closer approach to equilibrium during experiments at higher temperature. On the other hand, Riggs and Hurd [33] ascribed the decrease in activation at high levels of inhibition to the shift of the net corrosion reaction from that of the uncovered part on the substrate surface to the covered one.

Either the decrease or increase of the activation energy of the corrosion process could be explained in the light of the pre-exponential factor (λ) which is connected with the number of active centers in heterogeneous chemical reaction. The presence of adsorbed inhibitor molecules blocks a significant number of active sites on the surface which is energetically non-homogeneous. In general [34] the adsorbed inhibitor species block the most active sites, i.e. those with the lowest E_a values. Thus, sites which are greater in number (λ is of larger value in the presence of the inhibitor) take part in the subsequent corrosion process. However, values of λ were calculated and found to be 1.66×10^{14}, 1.45×10^{15}, 2.0×10^{23}, 1.41×10^{12} for the blank solution, $TMbPyBr_2$, $HMbPyBr_2$ and $MPhbPyCl_2$ respectively. The trend of λ values is similar to that observed for E_a values. The results can be explained by the fact that the presence of both $TMbPyBr_2$ and $HMbPyBr_2$ results in a high number of active centers remaining uncovered by the inhibitors. In the presence of $MPhbPyCl_2$, a low number of active centres remain uncovered by this compound.

According to the effect of temperature, inhibitors were classified into three groups [37]:

1. Inhibitors whose IE decreases with temperature increase; values of E_a are higher in the presence of the inhibitor than its absence.
2. Inhibitors whose IE does not change with temperature; values of E_a are approximately the same in the inhibited and uninhibited solutions.
3. Inhibitors whose IE increases with temperature increase; values of E_a are lower in the presence of the inhibitor than its absence.

The higher values of E_a in the presence of both $TMbPyBr_2$ and $HMbPyBr_2$ compared with that of the blank solution and the general decrease in IE% with increasing temperature are indicative of physical adsorption while chemisorption is suggested for adsorption of $MPhbPyCl_2$ (see below).

4.2 EIS measurements

The effect of temperature on the impedance behaviour of LCS in 0.5 M H_2SO_4 solution without and with 100 μM $TMbPyBr_2$ has been studied and the results are shown in Fig. 13a, b respectively. Impedance spectrum obtained for the pure medium (Fig. 13a) is similar to that obtained at 35 °C. Regardless of the inductive loop, the proposed equivalent circuit model is still valid. With increasing the temperature, the diameter of the capacitive loop is decreased. The parameters R_{ct} and Q_{dl} were calculated. Values of R_{ct} were found to be 20.6, 10.6, 4.8 and 4.7 Ω cm^2 at 25, 30, 35 and 40 °C respectively. The value of Q_{dl} obtained at 25 °C is $4.8 \times 10^{-4}\ \Omega^{-1}\ cm^{-2}\ s^n$ which gradually increases with rise in temperature reaching a value of $5.9 \times 10^{-4}\ \Omega^{-1}\ cm^{-2}\ s^n$ at the highest temperature. The decrease in R_{ct} and the increase in Q_{dl} indicate increased corrosion rate.

In the presence of 100 μM $TMbPyBr_2$ (Fig. 13b), values of R_{ct} are higher than that of the pure medium while those of Q_{dl} are lower, indicating the inhibition effect of this compound. Similar results were obtained for 250 μM $TMbPyBr_2$ and 100 μM $MPhbPyCl_2$. As a general behaviour the maximum value of R_{ct} is obtained at 35 °C.

The inhibition efficiencies were calculated from R_{ct} according to Eq. 7 and plotted as a function of temperature in Fig. 14, which is similar to Fig. 11 indicating that the results obtained from polarization curves and EIS are in good agreement.

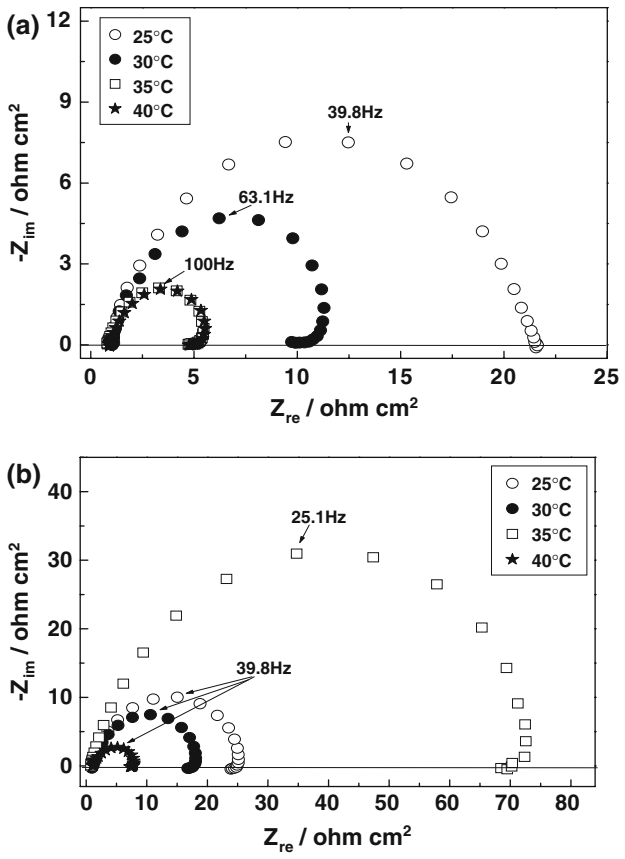

Fig. 13 Effect of temperature on Nequist plots of mild steel electrode recorded at E_{corr}: (**a**) in 0.5 M H_2SO_4 solution. (**b**) in presence of 100 μM $TMbPyBr_2$

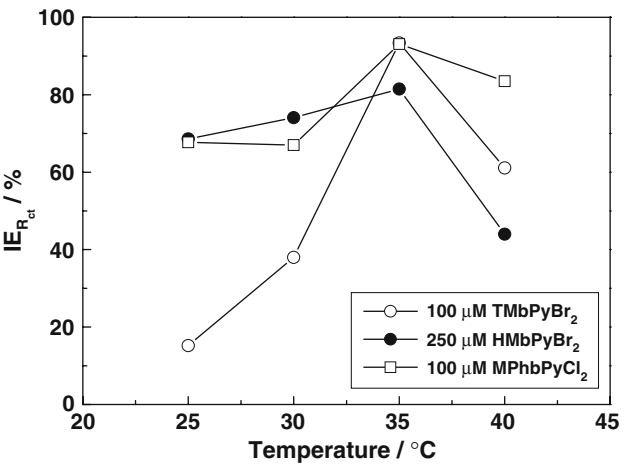

Fig. 14 Variation of the inhibition efficiency (deduced from R_{ct} values) of the bipyridinium salts at concentrations of maximum IE% with the temperature

5 Mechanism of corrosion inhibition and molecular structure—inhibition efficiency relationship

A plausible mechanism of corrosion inhibition of LCS in sulfuric acid solution by bipyridinium dihalides may be deduced on the basis of adsorption. The LCS surface attains a positive charge in aqueous H_2SO_4 solution as its potential of zero charge [38] ($E_{q=0}$ is −550 mV versus SCE) lies 24 mV more positive than its corrosion potential (E_{corr} = −526 mV versus SCE). So, adsorption of the

bipyridinium cations does not take place. As the solution contains either Cl^- or Br^- ions, these anions are firstly adsorbed followed by electrostatic attraction with the bipyridinium cations (physical adsorption).

Inhibition of both anodic and cathodic reactions (Fig. 3) can be explained as follows: under cathodic polarization conditions, the bipyridinium cations are adsorbed and block the cathodic sites of the surface and hence retard the hydrogen evolution reaction. On the other hand, adsorption of the cations on the anodic sites occurs via the π electrons of the two pyridine rings (planar adsorption orientation relative to the steel surface) giving rise to inhibition of the steel dissolution.

The difference in effectiveness can be attributed the difference in molecular structure. The dipyridinium compounds differ in the number of methyl groups attached to the pyridine ring where one $-CH_3$ group is attached to each pyridine ring of $TMbPyBr_2$ (in the 1 and 1' positions) and whereas two $-CH_3$ groups (in the 1, 1' and 2, 2' positions) are present in $HMbPyBr_2$. On the other hand, both $TMbPyBr_2$ and $HMbPyBr_2$ are N-methylated derivatives while $MPhbPyCl_2$ contains p-tolyl group attached to the hetero atom. It is well known that introduction of nucleophilic (electron donor) substituents, such as the methyl group, leads to increase of absorbability because of the increase of the π-electron density in the aromatic nucleus. Both polarization curves and EIS demonstrate that $HMbPyBr_2$ is the lease effective inhibitor since planar adsorption is not so strong and does not impart high inhibition efficiency. The presence of four methyl groups in the skeleton is expected to increase the electron density of the compound but the present results show that the increasing number of methyl groups is harmful because the steric effect exerted by these groups is dominant over their nucleophilc effect. The steric effect gives rise to weak adsorption (physical adsorption) and therefore low inhibition efficiency. This may also explain the low value of ΔG°_{ads} relative to those obtained for $TMbPyBr_2$ and $MPhbPyCl_2$ and the high value of E_a comparing to that of the pure medium. The steric hindrance of the two methyl groups in the 1 and 1' positions in $TMbPyBr_2$ is negligible compared to their donation effect; therefore $TMbPyBr_2$ gives better inhibition than $HMbPyBr_2$.

$MPhbPyCl_2$ is considered to be superior over $TMbPyBr_2$ although they have approximately the same IE% at 100 μM concentration (at 35 °C) for the following reasons:

(a) Value of ΔG^{o}_{ads} is higher for $MPhbPyCl_2$ than that of $TMbPyBr_2$.
(b) Values IE% of $MPhbPyCl_2$ obtained at −75 and 30 mV (Table 1) are higher than those of $TMbPyBr_2$.
(c) The slight decrease in the inhibition efficiency of $MPhbPyCl_2$ at 40 °C (Figs. 11 and 14).

The above-mentioned reasons indicate that $MPhbPyCl_2$ is chemisorbed on the steel surface. Such adsorption is exceptionally strong at 35 °C and greatly reduced the corrosion rate (enhancement of IE% as observed in Fig. 11 and that log i_{corr} values at 35 °C not follow the linear relationship of Fig. 12). The fact that the IE% increases with temperature is explained by Ammar and Alkhorafi [39] as the specific interaction between the iron surface and the inhibitor whereas others [35] consider the increase of IE% with temperature increase as the change in the nature of the adsorption mode, the inhibitor being physically adsorbed at lower temperatures, while chemisorption is favored as temperature increases.

The attachment of p-tolyl groups to the two hetero atoms of the pyridine rings extends the planar adsorption of $MPhbPyCl_2$ giving rise to blocking of greater surface area and hence preventing the electrode surface from contact with the corrosive medium. 3-(3-propylpyridine)-2-methylbenzothiazolium bromide (DBr) was found to provide better inhibition than 3-(3-carbomethyl)-2-methylbenzothiazolium bromide (CT) for mild steel corrosion in HCl solution because the DBr has greater surface area than CT [8].

6 Conclusions

Inhibition of LCS corrosion in 0.5 M H_2SO_4 solution by three bibyridinium dihalides was evaluated by electrochemical (potentiodynamic polarization and EIS) and surface analysis (SEM) techniques. The results revealed that:

(1) $TMbPyBr_2$ and $MPhbPyCl_2$ provide better inhibition effect than $HMbPyBr_2$ and $MPhbPyCl_2$ is the best compound.
(2) Potentiodynamic polarization curves proved that the bipyridinium salts act as inhibitors of mixed type and their adsorption surface obeys Langmuir adsorption isotherm.
(3) SEM investigation confirm the electrochemical results and the corrosion inhibition of LCS by $MPhbPyCl_2$ is a result of forming a compact surface layer
(4) EIS measurements indicate that charge transfer controls the corrosion of steel in 0.5 M H_2SO_4 solution in the absence and presence of bipyridinium compounds and the equivalent circuit $R_e(R_{ct}Q_{dl})$ represents the electrode/solution interface either at the corrosion potential or at −75 and 30 mV versus E_{corr}.
(5) From the EIS and polarization data in both concentration and temperature experiments the inhibitors can

be ranked as follows: $MPhbPyCl_2 > TMbPyBr_2 > HMbPyBr_2$.

(6) The compounds have maximum inhibition efficiency at 35 °C and their effectiveness declines at 40 °C.

References

1. Driver R, Meakins RJ (1977) Br Corros J 12:46
2. Frignani A, Zucchi F, Monticelli M (1983) Br Corros J 18:1
3. Frignani A, Tassinari M, Mészàros L, Trabanelli G (1991) Corros Sci 32:903
4. Frignani A, Monticelli C, Brunoro G, Trabanelli G (1985) Proc 6th Eur symp corros inhib (6SEIC), Ann Univ Ferrara, NS, Sez.V, Suppl 8:1519
5. Atia AA, Saleh MM (2003) J Appl Electrochem 33:171
6. Huang W, Zhao J (2006) Coll Surf A: Phys Eng Aspects 278:246
7. Popova A, Christov M, Vasilev A (2007) Corros Sci 49:3276
8. Popova A, Christov M, Vasilev A (2007) Corros Sci 49:3290
9. Lan CJ, Lee CY, Chin TS (2007) Electrochim Acta 52:5407
10. Hara M, Hashimoto K, Mashumoto T (1980, Electrochim Acta 25:1215
11. Subramaniam G, Balasubramanian K, Sridhar P (1990) Bull Electrochem 6:225
12. Qui L, Xie A, Shen Y (2004) Mater Chem Phys 87:237
13. Qui L, Xie A, Shen Y (2005) Corros Sci 47:273
14. Yao S, Jiang X, Zhou, Lv Y, Hu X (2007) Mater Chem Phys 104:301
15. Aziz SG, Obaid AY, Alyoubi AO, Abdel Fattah AA (1997) Corros Prevn Contl Dec:179
16. Obaid AY (1984) An electron spin resonance study of substituted bipyridinium radicals PhD thesis, University College, Cardiff, Wales
17. Evans AG, Evans JC, Nouri-Sorkhabi MH, Obaid AY, Rowlands CC (1985) J Chem Soc Perkin Trans 11:315
18. Morad MS (1999) J Appl Electrochem 29:619
19. Boukamp BA (1989) Report of University of Twente, CT88/265/128 and CT/89/214/128, The Netherland
20. Sham El Din AM, Mohammed RA, Haggag HH (1997) Desalination 114:85
21. Ashassi-Sorkhabi H, Ghalebsaz-Jeddi N (2006) Ultras Sonochem 13:180
22. Azambuja DS, Holzle LR, Muller IL, Piatnicki CMS (1999) Corros Sci 41:2083
23. Quartarone G, Zingales A, Bellomi T, Bortolato D, Capobianco G (2000) Proc 9th Eur symp corros inhib (9SEIC), Ann Univ Ferrara, NS, Sez V, Suppl 11, p 673
24. El-Awady AA, Abd-El-Nabey BA, Aziz SG (1992) J Electrochem Soc139:2149
25. Ashassi-Sorkabi H, Gahlebsaz-Jeddi N, Hashemzadeh F, Jahani H (2006) Electrochim Acta 51:3848
26. Kustu C, Emregul KC, Atakol O (2007) Corros Sci 49:2800
27. Lebrini M, Lagrenee M, Vezin H, Traisnel M, Bentiss F (2007) Corros Sci 49:2254
28. Lebrini M, Traisnel M, Lagrenee M, Mernari B, Bentiss F (2007) Corros Sci, doi:101016/jcorsci200705031
29. Niu L, Zhang H, Wei F, Wu S, Cao X, Liu P (2005) Appl Surf Sci 252:1634 (References therein)
30. Juttner K (1990) Electrochim Acta 35:1501
31. Bentiss F, Lebrini M, Vezin H, Lagrenee M (2004) Mater Chem Phys 87:18
32. Marin-Cruz J, Cabrera-Sierra R, Pech-Canul MA, Gonzalez I (2006) Electrochim Acta 51:1847
33. Riggs OL, Hurd RM (1967) Corrosion 23:252
34. Popova A, Sokalova E, Raicheva S, Christova M (2003) Corros Sci 45:33 (References therein)
35. Bentiss F, Lebrini M, Lagrenee M (2005) Corros Sci 47:2915 (References therein)
36. Hoar TP, Holliday RD (1953) J Appl Chem 3:502
37. Radovici O (1965) Proc 2th Eur symp corros inhib (2SEIC), Ann Univ Ferrara:178
38. Morad MS (2007) J Appl Electrochem 37:661
39. Ammar IA, El Khorafi FM (1973) Werkst Korros 24:702